Oxygen vacancy segregation in grain boundaries of $BaZrO_3$ using interatomic potentials

Anders Lindman, Edit E. Helgee, B. Joakim Nyman, Göran Wahnström*

Department of Applied Physics, Chalmers University of Technology, SE-41296 Göteborg, Sweden

Abstract

We have used classical interatomic potentials to determine the structure, interface energy and oxygen vacancy segregation energies of eight different grain boundaries (GBs) in $BaZrO_3$ with tilt axis $[\bar{1}10]$. Two of these have been studied previously with density functional theory and the agreement is satisfactory. The results suggest that oxygen vacancies prefer to reside near the boundary interface for all these GBs. The minimum segregation energies range between $-1.86\,\mathrm{eV}$ and $-0.57\,\mathrm{eV}$, and the typical core width is about 10 Å. The resulting depletion layers have been evaluated using a thermodynamic space-charge model. Space-charge potential barriers between 0.2-0.8 eV were obtained with dopant concentrations of 5 % and 10 %.

Keywords: $BaZrO_3$, Grain boundary, Space-charge model, Interatomic potential, Oxygen vacancy segregation

1. Introduction

Acceptor-doped $BaZrO_3$ shows great promise as an electrolyte for proton conducting intermediate temperature SOFCs due to that it is chemically stable and exhibits high bulk conductivity [1, 2]. Polycrystalline samples do however display significantly lower conductivity which is caused by resistive grain boundaries (GBs) [1, 3, 4]. This has recently been interpreted in terms of the space-charge model by several research groups [5–13]. This model assumes that positively charged defects, such as oxygen vacancies, accumulate at the GB core and thereby give rise to an electrostatic potential. In turn, the potential depletes the nearby regions of positively charged defects, resulting in depletion layers next to the core [14]. This reduces the proton concentration near the GB which lowers the conductivity.

For the accumulation to occur the defect formation energies need to be lower at the GB core. Previous studies by our group on a tilt grain boundary in $BaZrO_3$ using density-functional theory (DFT) suggest that vacancies do segregate to the GB core [13]. For a more comprehensive understanding more GB structures have to be considered. The number of GBs that can be treated with DFT is very limited due to the high computational cost for large systems. In order to study more complex GB structures less time consuming methods are therefore needed.

We have studied eight different tilt grain boundaries in $BaZrO_3$ with tilt axis $[\bar{1}10]$ using classical interatomic potentials. The grain boundary energy as well as oxygen vacancy segregation energies have been determined for each GB. These segregation energies were then used as input to a thermodynamic space-charge model in order to determine the corresponding space-charge potentials. Only dry conditions are treated which means that the defects present in the simulations are oxygen vacancies and acceptor dopants, where the latter are assumed to be immobile. During doping and hydration processes there is also the possibility that holes are formed instead of oxygen vacancies and/or hydroxide ions [15, 16]. In this study however we assume that the formation of holes can be neglected.

2. Theory

To determine the equilibrium distribution of defects within a material we need the electrochemical potential of each defect species. For the electrochemical potential of species n we use the expression

$$\mu_n(z) = \mu_n^\circ(z) + q_n e\varphi(z) + k_\mathrm{B}T \ln \frac{c_n(z)}{c_n^{\max}(z) - c_n(z)} \quad (1)$$

where $\mu_n^\circ(z)$ is the standard chemical potential, q_n is the effective charge of the defect, e is the elementary charge, $\varphi(z)$ is the electrostatic potential, $c_n(z)$ is the defect concentration and $c_n^{\max}(z)$ is the concentration of possible defect sites. The spatial coordinate z is chosen so that the grain boundary plane is located at $z = 0$ and the grain interior at $z = \pm\infty$. The defect species considered in this work are oxygen vacancies with $q = +2$ and acceptor dopants with $q = -1$. The vacancy and dopant concentrations are denoted $c_\mathrm{V}(z)$ and $c_\mathrm{A}(z)$ respectively. The dopant ions are assumed to be immobile and evenly distributed in the

*Corresponding author. Tel.: +46 (0)31 7723634

Email address: goran.wahnstrom@chalmers.se (Göran Wahnström)

material, i.e. $c_{\mathrm{A}}(z) = c_{\mathrm{A}}(\infty)$. From here on the dopant concentration will be referred to as c_{A}.

The electrostatic potential in Eq. 1 is given by Poisson's equation

$$\frac{\mathrm{d}^2\varphi(z)}{\mathrm{d}z^2} = -\frac{\rho(z)}{\epsilon_{\mathrm{r}}\epsilon_0} \tag{2}$$

where $\rho(z)$ is charge density and ϵ_{r} is the dielectric constant. With oxygen vacancies and acceptor dopants $\rho(z)$ is given by

$$\rho(z) = 2ec_{\mathrm{V}}(z) - ec_{\mathrm{A}} \tag{3}$$

The grain interior is charge neutral, and thereby Eq. 3 yields the condition $c_{\mathrm{V}}(\infty) = c_{\mathrm{A}}/2$.

We make the assumption that the GB region is in equilibrium with the grain interior. This assumption yields the equilibrium equation $\mu_{\mathrm{V}}(z) = \mu_{\mathrm{V}}(\infty)$, which together with Eq. 1 can be written as

$$\begin{aligned}\Delta\mu^{\circ}_{\mathrm{V}}(z) + 2e\Delta\varphi(z) + k_{\mathrm{B}}T\ln\frac{c_{\mathrm{V}}(z)}{c^{\max}_{\mathrm{V}}(z) - c_{\mathrm{V}}(z)} \\ = k_{\mathrm{B}}T\ln\frac{c_{\mathrm{V}}(\infty)}{c^{\max}_{\mathrm{V}}(\infty) - c_{\mathrm{V}}(\infty)}\end{aligned} \tag{4}$$

where $\Delta\mu^{\circ}_{\mathrm{V}}(z) = \mu^{\circ}_{\mathrm{V}}(z) - \mu^{\circ}_{\mathrm{V}}(\infty)$ and $\Delta\varphi(z) = \varphi(z) - \varphi(\infty)$.

As will be shown further on in the paper, there can be two or more defect sites at the same z-coordinate with different values of $\Delta\mu^{\circ}_{\mathrm{V}}(z)$ within the grain boundary region. Assuming there are i different sites, we then have to solve Eq. 4 for each value $\Delta\mu^{\circ}_{\mathrm{V},i}(z)$ with corresponding $c^{\max}_{\mathrm{V},i}(z)$ to obtain the defect concentration at each site, $c_{\mathrm{V},i}(z)$. The total defect concentration is given by $c_{\mathrm{V}}(z) = \sum_i c_{\mathrm{V},i}(z)$.

3. Computational details

3.1. Interatomic potential

To model the grain boundary structures we use interatomic pair potentials of the form

$$U_{ij}(r) = A_{ij}\exp\left(-\frac{r}{\rho_{ij}}\right) - \frac{C_{ij}}{r^6} + \frac{q_iq_j}{r} \tag{5}$$

where q_i and q_j are the charges of the ions and A_{ij}, ρ_{ij} and C_{ij} are empirical parameters. The first two terms, which correspond to Pauli and van der Waals interaction, are short ranged and they were truncated with a cut-off radius of 6 Å [17]. This choice yields errors in grain boundary energy below 1 % suggesting sufficient accuracy. The last term, which is the Coulomb interaction, is long ranged and is calculated using the Ewald summation technique. This description is denoted the rigid ion model (RIM).

Polarizability has been included through the use of the shell model (SM) [18]. The ions are seen as consisting of a core and a massless shell which are connected through a harmonic spring. The core and the shell both have a charge which when added together are equal to the formal charge of the ion. The polarizability is then given by $\alpha = q_s^2/k_s$ where q_s is the shell charge and k_s the force constant of the spring.

Table 1: The unrelaxed structure dimensions and the number of atoms for $[\bar{1}10]$ tilt grain boundary supercells of $BaZrO_3$. The third axis corresponds to the grain boundary plane. $a_0 = 4.191$ Å.

Axes	Dimensions	No. of atoms
$[11\bar{2}], [\bar{1}10], [111]$	$2\sqrt{6}a_0 \times 3\sqrt{2}a_0 \times 8\sqrt{3}a_0$	1440
$[11\bar{1}], [\bar{1}10], [112]$	$2\sqrt{3}a_0 \times 3\sqrt{2}a_0 \times 6\sqrt{6}a_0$	1080
$[33\bar{2}], [\bar{1}10], [113]$	$\sqrt{22}a_0 \times 3\sqrt{2}a_0 \times 6\sqrt{11}a_0$	1980
$[22\bar{1}], [\bar{1}10], [114]$	$2\sqrt{9}a_0 \times 3\sqrt{2}a_0 \times 4\sqrt{18}a_0$	2160
$[55\bar{2}], [\bar{1}10], [115]$	$\sqrt{54}a_0 \times 3\sqrt{2}a_0 \times 12\sqrt{3}a_0$	3240
$[33\bar{1}], [\bar{1}10], [116]$	$\sqrt{19}a_0 \times 3\sqrt{2}a_0 \times 3\sqrt{38}a_0$	1710
$[77\bar{2}], [\bar{1}10], [117]$	$\sqrt{102}a_0 \times 3\sqrt{2}a_0 \times 2\sqrt{51}a_0$	3060
$[44\bar{1}], [\bar{1}10], [118]$	$\sqrt{33}a_0 \times 3\sqrt{2}a_0 \times 2\sqrt{66}a_0$	1980

All calculations with the interatomic potential were performed using the DL_POLY program package [19]. The parameters we used for the simulations are the same as those used by Stokes and Islam [20]. This set of parameters gave a lattice constant of 4.191 Å, both with and without polarizability, which is the same as the experimental value [21].

Eight different stoichiometric tilt grain boundaries with the rotational axis $[\bar{1}10]$ have been considered. The GBs are denoted $(11k)$, $k = 1, \ldots, 8$, which corresponds to the interface plane of each GB. The initial structures of the grain boundary supercells were chosen to be symmetric tilt grain boundaries of the considered orientations. The supercell was chosen so that a bulk supercell with the same dimensions, the same number of ions and a periodic structure of the same orientation could be constructed. A convergence test of the (111) GB indicated that in order to obtain non-interacting boundaries the cell needs to be at least 50 Å in the direction perpendicular to the GB plane. More detailed information about these structures is shown in Tab. 1.

The incorporation of the shell model makes the simulations more computationally demanding. The relaxed structures of the simulations performed without polarizability therefore served as initial structures for the shell model simulations.

The structural optimization of the GBs was performed using a combination of the conjugate gradient (CG) method and molecular dynamics (MD) simulations. The NσT ensemble was used in the MD simulations with the restriction that the supercell was allowed to change only in the direction perpendicular to the grain boundary plane. The MD simulations were started at temperatures around 500 K. The system was first equilibrated with MD and then the ionic positions were relaxed using the CG method. The procedure was repeated several times and temperature was reduced in steps of about 50 K to zero temperature. A final, fully relaxed, structure was obtained and we verified

that the two different GBs in the supercell were essentially structurally identical.

To calculate the change in energy due to the formation of a vacancy only the CG method was used. An oxygen ion was removed and the structure was relaxed. The CG method finds local minima which corresponded to that only ions in the vicinity of the vacancy moved substantially. To maintain a charge neutral system a uniform background charge was introduced, which has the same magnitude but opposite sign as the vacancy.

3.2. Space-charge calculations

To determine the equilibrium concentrations and the corresponding space-charge potentials Eq. 2 and 4 are solved iteratively until $\Delta\varphi(z)$ and $c_{\mathrm{V}}(z)$ converge into a steady-state solution. The grain boundary region is represented by a uniform numerical grid where the grain interior is located at $|z| > z_{\max} = 80\,\text{Å}$. We have used the following boundary conditions to obtain a proper solution: $\Delta\varphi(\pm z_{\max}) = 0$, $\Delta\varphi'(\pm z_{\max}) = 0$ and $c_{\mathrm{V}}(\pm z_{\max}) = c_{\mathrm{A}}/2$.

Inside the grain boundary core, $|z| < w_c/2$, where w_c is the core width, we will assume that $\Delta\mu^{\circ}_{\mathrm{V},i}(z) \neq 0$. The vacancy concentration of each site i is determined from Eq. 4 and the resulting charge density is spread out uniformly inside the grain boundary core, $|z| < w_c/2$. For $|z| > w_c/2$ we assume that the vacancy formation energy is the same for all sites and hence $\Delta\mu^{\circ}_{\mathrm{V}}(z) = 0$.

We have used $\epsilon_{\mathrm{r}} = 75$ for all space-charge simulations. This value is representative for experimental data on Y-doped $BaZrO_3$ [6].

4. Results & discussion

4.1. Grain boundary structures and segregation energies

Converged structures were obtained for all eight grain boundaries. During the relaxation procedure, all but the (111) GB were displaced from the initial symmetric configuration. The displacement was in all cases on the order of 2 Å and perpendicular to the $[\bar{1}10]$ direction. This is a consequence of the short distance between barium ions at the boundary interface in the initial symmetric configuration.

With these structures we determined the grain boundary energy γ_{gb}. It is defined as

$$\gamma_{\mathrm{gb}} = \frac{E^{\mathrm{tot}}_{\mathrm{gb}} - E^{\mathrm{tot}}_{\mathrm{bulk}}}{2A}, \tag{6}$$

where $E^{\mathrm{tot}}_{\mathrm{gb}}$ is the energy of the grain boundary supercell, $E^{\mathrm{tot}}_{\mathrm{bulk}}$ is the energy of the bulk supercell and A is the area of the grain boundary interface. The factor of $1/2$ is included due to the presence of two grain boundaries in the supercell. Results are given in Tab. 2 together with the grain boundary expansion in the direction perpendicular to the grain boundary plane, Δ_{gb}. The values of γ_{gb} in the table are small enough to suggest that all GBs could be formed in a real sample. In Tab. 2 we have listed results for the (111) and (112) GBs from DFT calculations [22]. The results suggest that the interatomic potential gives a satisfactory description. The inclusion of polarizability does not generally improve γ_{gb} and Δ_{gb}. Similar behavior has been observed for shell model calculations of grain boundaries in $SrTiO_3$ [23].

To determine if oxygen vacancies segregate we calculated the segregation energy for the vacancies. The vacancy segregation energy ΔE_{V} is defined as the difference in formation energy between a vacancy in the vicinity of a grain boundary and a vacancy in a reference state. The reference state should represent a vacancy in the grain interior and is therefore chosen to be a vacancy site positioned as far away as possible from the grain boundary in the supercell. ΔE_{V} can then be determined by

$$\Delta E_{\mathrm{V}} = E^{\mathrm{tot}}_{\mathrm{gb,V}} - E^{\mathrm{tot}}_{\mathrm{gb,V_{ref}}} \tag{7}$$

where $E^{\mathrm{tot}}_{\mathrm{gb,V}}$ is the energy of a GB supercell with a vacancy and $E^{\mathrm{tot}}_{\mathrm{gb,V_{ref}}}$ is the energy of a GB supercell with a vacancy in the reference state.

In Fig. 1 we show the segregation energy for all vacancies within ±15 Å of the GB plane for all eight GB orientations. For all boundaries the formation energy of vacancies within a distance of approximately ±5 Å from the GB plane is strongly affected. Both positive (more strongly bound oxygen ions) and negative (less strongly bound oxygen ions) segregation energies are obtained. Considering these results we define the grain boundary core region to be $|z| < w_c/2 = 5\,\text{Å}$. This region is marked by dashed lines in the figure. The largest tendency for segregation is given by the minimum value of the segregation energy $\Delta E^{\mathrm{min}}_{\mathrm{V}}$, and the corresponding value for each GB is given in Tab. 2. These energies range from $-1.86\,\text{eV}$ to $-0.57\,\text{eV}$, with most lower than $-1\,\text{eV}$. This indicates that it is much more favorable for oxygen vacancies to reside near the grain boundary rather than in the grain interior. We also notice that the values obtained with polarizability included are in better agreement with DFT, and therefore these values will be used in the space-charge calculations below.

Another feature seen in Fig. 1 is that there are two types of vacancy site distributions. In the (111) and (112) GBs, which have high tilt angles, the vacancy density of sites (VDOS) in the core region corresponds to two sorts, one with negative segregation energy and one with positive. In the other six GBs with lower tilt angles, the VDOS is more uniformly distributed in energy. In Fig. 2 the cumulative VDOS for these six boundaries are shown. For all these boundaries the cumulative VDOS shows a roughly linear trend for negative segregation energies, which corresponds to a constant VDOS in that region. In previous studies with space-charge models where core segregation is included usually only one segregation energy is considered, which is most similar to the distribution in the (111) and (112) GBs [12, 13, 24].

Table 2: The grain boundary energy γ_{gb}, expansion Δ_{gb} and minimum segregation energy $\Delta E_{\mathrm{V}}^{\mathrm{min}}$ of $[\bar{1}10]$ tilt grain boundaries in $BaZrO_3$ obtained with the rigid ion model (RIM) and with polarizability included through the shell model (SM). For the (111) and (112) grain boundaries corresponding results from DFT calculations are also shown [22].

GB	γ_{gb} (J/m^2)			Δ_{gb} (Å)			$\Delta E_{\mathrm{V}}^{\mathrm{min}}$ (eV)		
	RIM	SM	DFT	RIM	SM	DFT	RIM	SM	DFT
(111)	0.60	0.56	0.51	0.20	0.20	0.20	−1.41	−1.09	−0.65
(112)	0.86	0.73	0.93	0.42	0.42	0.45	−0.81	−0.57	−0.52
(113)	1.24	1.10		1.57	1.57		−1.61	−1.23	
(114)	1.25	1.11		1.09	1.09		−1.38	−1.10	
(115)	1.50	1.31		1.71	1.71		−1.52	−1.38	
(116)	1.56	1.40		1.24	1.24		−1.51	−1.32	
(117)	1.71	1.52		1.75	1.71		−1.82	−1.86	
(118)	1.72	1.55		1.32	1.32		−1.66	−1.62	

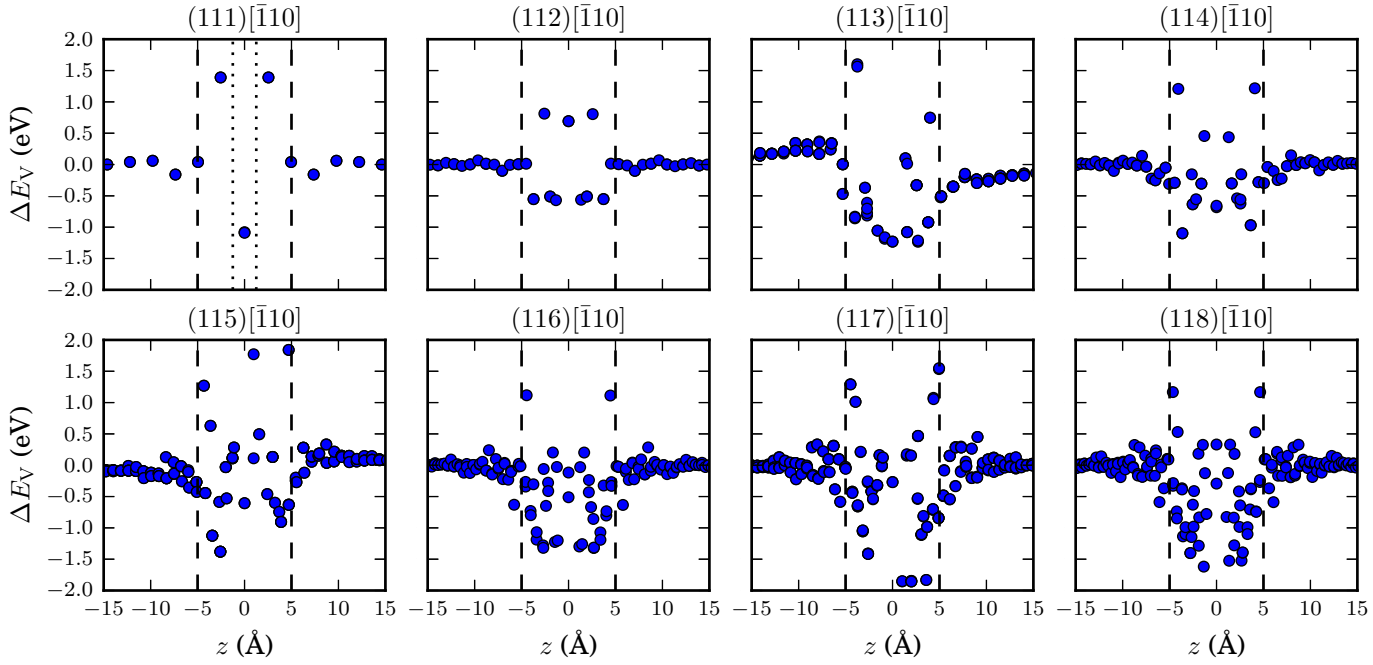

Figure 1: The vacancy segregation energies of all vacancy sites within a distance of ±15 Å from the grain boundary plane for each grain boundary orientation. All shown values are obtained using the shell model (SM). The dashed lines mark the grain boundary core region with a core width $w_c = 10$ Å, while the dotted lines in the (111) GB mark a core region with $w_c = 2.5$ Å.

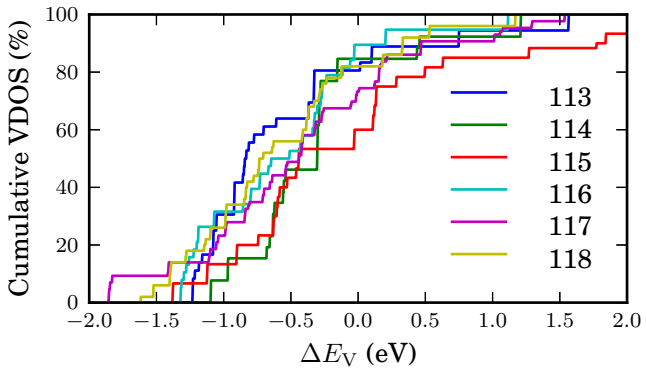

Figure 2: The cumulative oxygen vacancy density of sites (VDOS) of the $(11k), k = 3, \ldots, 8$, grain boundaries.

Table 3: The space-charge potential height $\Delta\varphi(0)$ and the core charge Q_c for the different grain boundaries at $T = 600\,\mathrm{K}$. Values are shown for dopant concentrations of 5 % and 10 %. The core width w_c used in the simulations is $w_c = 10\,\text{Å}$ (a: $w_c = 2.5\,\text{Å}$).

GB	$\Delta\varphi(0)$ (V)		Q_c (Cm^{-2})	
	5 %	10 %	5 %	10 %
(111)[a]	0.47	0.48	0.48	0.68
(111)	0.48	0.48	0.47	0.66
(112)	0.23	0.24	0.31	0.43
(113)	0.52	0.53	0.49	0.69
(114)	0.44	0.44	0.45	0.61
(115)	0.55	0.53	0.50	0.67
(116)	0.57	0.58	0.52	0.72
(117)	0.80	0.76	0.62	0.82
(118)	0.65	0.64	0.55	0.76

4.2. Space-charge calculations

The values of ΔE_V obtained with the shell model were used to represent $\Delta\mu_V^\circ(z)$ in all space-charge simulations. Tab. 3 shows the values of $\Delta\varphi(0)$ and the total core charge Q_c obtained from calculations made with dopant concentrations of 5 % and 10 %. With 5 % $\Delta\varphi(0)$ ranges from 0.23-0.80 V and Q_c from 0.31-0.62 Cm^{-2}. These values are comparable to results for 5 % Y-doped $BaZrO_3$ determined experimentally under similar conditions [6–8, 10]. If we compare the values of Q_c with the values of $\Delta E_V^{\min}$ in Tab. 2 we find that stronger segregation gives rise to a larger core charge.

The core width w_c is a parameter based on the distribution of low-energy vacancy sites seen in Fig. 1. For all GBs except the (111) it was appropriate to chose $w_c = 10\,\text{Å}$. To investigate how this choice affects the space-charge potentials we carried out simulations of the (111) GB with two different core widths, 2.5 Å and 10 Å. The simulations were performed for both 5 % and 10 % dopant concentration and the results are given in Tab. 3. The results show that the value of w_c barely affects $\Delta\varphi(0)$ and Q_c, which suggests that an accurate choice of w_c is not of great importance. However, the space-charge properties of the GB are mainly determined by the low energy vacancy sites which implies that w_c needs to be large enough so that these sites are accounted for within the core region.

In the simulations the dopant ions are assumed to be immobile. Recent experiments show that dopant segregation to the grain boundary can increase the grain boundary conductivity significantly [10]. If dopants were mobile then they could enter the core and the surrounding space-charge layers, and thereby reduce the space-charge potential. However, vacancies could respond to this reduction since they also are mobile. This could lead to an increase of vacancies in the core that counteract the dopants, provided that the low energy vacancy sites are not saturated.

With mobile dopants we found [22] that for the (111) GB dopants segregate both to the core and space-charge layers but the space-charge potential height remains rather unchanged. This is due to that there is no saturation of the low energy vacancy sites. The width of the potential is slightly decreased which reduces the width of the space-charge layers, and this is related to the increased dopant concentration in the space-charge layers. Our results regarding the barrier height differ with respect to results reported by De Souza [24]. He found through similar theoretical modeling that dopant segregation to the core saturates the vacancy sites and thereby reduces the space-charge potential. However, he uses a vacancy site concentration of $1 \cdot 10^{18}\,\mathrm{m}^{-2}$ in the core which is one order of magnitude lower than the concentration we obtained, which is $1 \cdot 10^{19}\,\mathrm{m}^{-2}$ (corresponds to the data point with $\Delta E_V = -1.09\,\mathrm{eV}$ in Fig. 1).

For the (117) GB, where there are sites with different energy that favor segregation, we found [22] that the space-charge potential is reduced by about 0.2 eV when dopants segregate to the core and the space-charge layers. The width of the potential and the space-charge layers was reduced as well. This is more in line with De Souza's results [24], and the reduction of the potential is related to that the concentration of sites with the minimum energy is lower compared to the (111) GB, $3 \cdot 10^{18}\,\mathrm{m}^{-2}$ (corresponding to the three data points with $\Delta E_V \approx -1.85\,\mathrm{eV}$ in Fig. 1), and they become saturated. However, there are still available sites for vacancy segregation but with higher energy and therefore less likely to become occupied.

It also important to note the fact that the results we present regarding mobile dopants [22] are obtained under the assumption that the dopants have zero segregation energy, which means that the driving force for dopant segregation is solely determined by the space-charge potential. A finite dopant segregation energy could affect the space-charge potential in several ways depending on its magnitude and sign.

Another important restriction is the use of Eq. 1 for the electrochemical potential. The only considered defect-defect interaction in Eq. 1 is electrostatic which is incorporated through the mean-field Poisson equation. At high vacancy concentrations in the core defect interactions which are not accounted for are likely to become important. If

the vacancy concentration increases then it is possible that such interactions make further vacancy segregation less favorable which would lead to a reduction of the space-charge potential.

Finally, we only consider dry conditions. In wet conditions there is also the possibility that protons could affect the space-charge potential. We have previously considered wet conditions with the restriction of a proton free core region [13]. This study suggests that protons reduce the potential at low temperatures. Additionally, recent DFT calculations carried out by our group [25] do suggest that proton segregation is favorable, and it may increase the potential barrier.

5. Conclusions

We have determined the structure and oxygen vacancy segregation energy of eight different tilt grain boundaries (GBs) in $BaZrO_3$ using classical interatomic pair potentials. We found that vacancies tend to segregate in all the GBs with minimum segregation energies in the range between $-1.86\,\mathrm{eV}$ and $-0.57\,\mathrm{eV}$, and the typical core width is about $10\,\text{Å}$. We carried out simulations both with and without polarizability, which was introduced through the shell model. We have compared our results with recent density-functional theory (DFT) calculations. We found that the shell model did not improve over the rigid ion model on the grain boundary energy and expansion in general, but the segregation energies were in better agreement with DFT. In the (111) and (112) GBs, which are high-angle tilt GBs, all vacancy sites that favor segregation correspond to the minimum segregation energy. In the $(11k), k = 3, \ldots, 8$, GBs, which have lower tilt angles, there is a distribution of sites with different segregation energy in the grain boundary core that favor segregation.

Space-charge calculations with the obtained segregation energies and with the assumption of immobile dopants resulted in electrostatic potentials at the GB interface. Potential barriers between 0.2-0.8 V were obtained with dopant concentrations of 5 % and 10 %. Our results are discussed in connection to the possibility of mobile dopants.

We would like to acknowledge SNIC for computational resources and the Swedish Energy Agency for financial support.

References

[1] K. D. Kreuer, Annu. Rev. Mater. Res. 33 (2003) 333.
[2] E. Fabbri, L. Bi, D. Pergolesi, E. Traversa, Adv. Mater. 24 (2011) 195.
[3] K. D. Kreuer, Solid State Ionics 125 (1999) 285.
[4] H. G. Bohn, T. Schober, J. Am. Ceram. Soc. 83 (2000) 768.
[5] C. Kjølseth, H. Fjeld, Ø. Prytz, P. I. Dahl, C. Estournès, R. Haugsrud, T. Norby, Solid State Ionics 181 (2010) 268.
[6] C. Chen, C. E. Danel, S. Kim, J. Mater. Chem. 21 (2011) 5435.
[7] F. Iguchi, N. Sata, H. Yugami, J. Mater. Chem. 20 (2010) 6265.
[8] F. Iguchi, C. Chen, H. Yugami, S. Kim, J. Mater. Chem. 21 (2011) 16517.
[9] M. Shirpour, R. Merkle, C. T. Lin, J. Maier, Phys. Chem. Chem. Phys. 14 (2011) 730.
[10] M. Shirpour, B. Rahmati, W. Sigle, P. A. van Aken, R. Merkle, J. Maier, J. Phys. Chem. C 116 (2012) 2453.
[11] M. Shirpour, R. Merkle, J. Maier, Solid State Ionics 216 (2012) 1.
[12] R. A. De Souza, Z. A. Munir, S. Kim, M. Martin, Solid State Ionics 196 (2011) 1.
[13] B. J. Nyman, E. E. Helgee, G. Wahnström, Appl. Phys. Lett. 100 (2012) 061903.
[14] J. Maier, Prog. Solid State Chem. 23 (1995) 171.
[15] K. Nomura, H. Kageyama, Solid State Ionics 178 (2007) 661.
[16] Y. Yamazaki, C. Yang, S. M. Haile, Scripta Materialia 65 (2011) 102.
[17] G. V. Lewis, C. R. A. Catlow, J. Phys. C: Solid State Phys. 18 (1985) 1149.
[18] B. G. Dick, A. W. Overhauser, Phys. Rev. 112 (1958) 90.
[19] W. Smith, T. R. Forester, I. T. Todorov, The dl_poly_2 user manual, 2009. Http://www.cse.scitech.ac.uk/ccg/software /DL_POLY.
[20] S. J. Stokes, M. S. Islam, J. Mater. Chem. 20 (2010) 6258.
[21] W. Pies, A. Weiss, Landolt-Börnstein: Numerical data and functional relationships in science and technology, volume 7e, Springer, Berlin, 1975.
[22] E. E. Helgee, A. Lindman, B. J. Nyman, G. Wahnström (in preparation).
[23] N. A. Benedek, A. L. Chua, C. Elsässer, A. P. Sutton, M. W. Finnis, Phys. Rev. B 78 (2008) 064110.
[24] R. A. De Souza, Phys. Chem. Chem. Phys. 11 (2009) 9939.
[25] E. E. Helgee, A. Lindman, G. Wahnström, Fuel Cells (submitted).